EARTH SURFACE PROCESSES AND LANDFORMS
Earth Surf. Process. Landforms **46**, 430–442 (2021)

Published online 5 December 2020 in Wiley Online Library
(wileyonlinelibrary.com) DOI: 10.1002/esp.5035

Sediment cascades and the entangled relationship between human impact and natural dynamics at the pre-pottery Neolithic site of Göbekli Tepe, Anatolia

Moritz Nykamp,[1]* Fabian Becker,[1] Ricarda Braun,[2] Nadja Pöllath,[3] Daniel Knitter,[2] Joris Peters[3,4] and Brigitta Schütt[1]

[1] Institute of Geographical Sciences, Freie Universität Berlin, Berlin 12249, Germany
[2] Institute of Geography, Christian-Albrechts-Universität zu Kiel, Kiel 24118, Germany
[3] Section Palaeoanatomy, SNSB, Staatssammlung für Anthropologie und Paläoanatomie, München 80539, Germany
[4] Veterinary Sciences Department, Ludwig-Maximilians-Universität München, München 80539, Germany

Received 28 April 2020; Revised 2 November 2020; Accepted 3 November 2020

*Correspondence to: Moritz Nykamp, Institute of Geographical Sciences, Freie Universität Berlin, Malteserstr. 74-100, 12249 Berlin, Germany.
E-mail: m.nykamp@fu-berlin.de

ESPL
Earth Surface Processes and Landforms

ABSTRACT: This study presents a meta-analysis of radiocarbon ages for the environs of Göbekli Tepe – one of the oldest monumental structures worldwide – using cumulative probability functions to diachronically assess phases of geomorphodynamic activity as controlled by natural or anthropogenic drivers. We employ *sediment cascades* as a heuristic framework to study the complex responses of the geomorphological system to various triggers at local to supra-regional scales. Possible triggers include climatic variability as documented by supra-regional hydroclimatic proxy data, regional demographic trends, and local to regional socioeconomic developments such as the emergence of sedentism or the introduction and dispersal of livestock herding. Our results show that phases of intensified geomorphodynamic activity occurred between ca. 7.4–7.0 and 5.8–3.3 ka BP. These phases roughly coincide with phases of population growth in southern Turkey and climatic variations in Turkey and the Levant. The phase between ca. 5.8–3.3 ka BP also corresponds to the time when organized agriculture and the seeder plough were introduced. Also, the identified phases are in agreement with the general trend of varying geomorphodynamic activity in the Eastern Mediterranean as driven by human impact and climatic change. However, neither the Younger Dryas–Holocene transition nor the development of herding during the Pre-Pottery Neolithic left a clear signature. We demonstrate how the different depositional environments in the studied landscape compartments vary with respect to their spatiotemporal coverage and discuss challenges when trying to understand processes that once shaped landscapes of past societies. © 2020 The Authors. Earth Surface Processes and Landforms published by John Wiley & Sons Ltd

KEYWORDS: Holocene geomorphodynamic activity; cumulative probability functions of ^{14}C ages; human–environment interactions; geoarchaeology; sediment connectivity

Introduction

Sediment cascades are a characterizing feature of geomorphological systems, illustrating the complex interplay between erosion, transport, and accumulation (Bracken *et al.*, 2015). Such systems comprise a set of interlinked subsystems at various scales and of varying complexity, forming a nested hierarchy (Chorley and Kennedy, 1971; Harvey, 2002). External forces controlling such systems include climatic variability, (short-term) environmental changes, and human impact. These, together with system-inherent geomorphological thresholds, lead to complex system responses at different spatial and temporal scales (Schumm, 1973; Lang and Hönscheidt, 1999; Brierley *et al.*, 2006; Fuchs *et al.*, 2011; Houben *et al.*, 2012; Bracken *et al.*, 2015). Due to the complexity of both geomorphological and cultural systems and their nonlinear relationships, understanding landscape evolution is challenging (Schumm, 1991; Poeppl *et al.*, 2017).

Göbekli Tepe, located in Upper Mesopotamia (semi-arid southeastern Turkey; Figure 1A), is one of the oldest known monumental structures worldwide, dating from the mid-12th to the end of the 10th millennium BP. Its occupation period covers more than half of the so-called Pre-Pottery Neolithic (PPN) period, more precisely its earlier phase, termed PPN A, and the first half of its later phase, named PPN B (see Figure 3 for comparison of geochronological periods and cultural

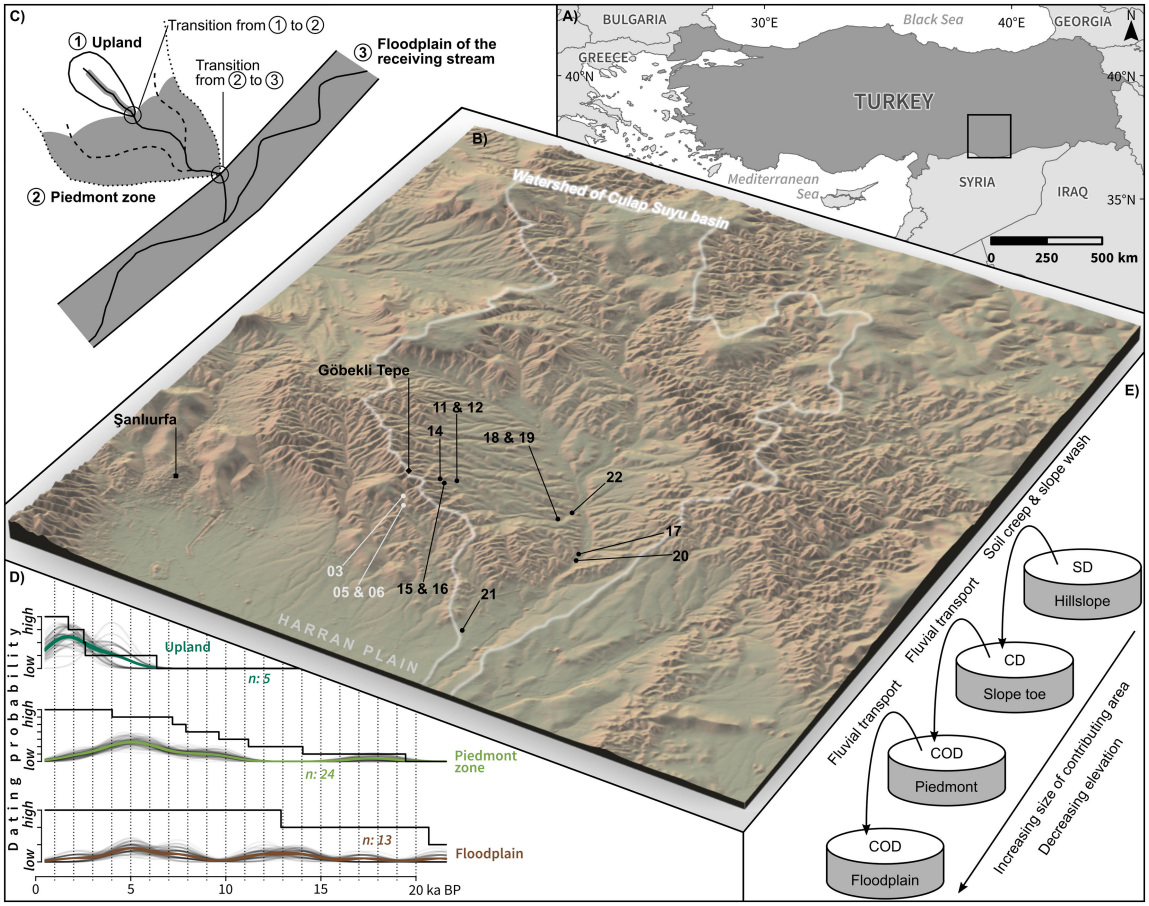

Figure 1. (A) Overview map showing the study site in southeastern Turkey. (B) Regional overview. Locations sampled along the sediment cascade within the Culap Suyu basin are illustrated in black; those located in the identified landscape compartments but situated beyond the catchment area are illustrated in grey. 3D illustration is based on TanDEM-X elevation data with 12 m × 12 m pixel size, ©DLR 2017. (C) Conceptual visualization of the three landscape compartments (indicated by 1–3) that form the studied sediment cascade. Grey colours indicate the characteristic deposits observed in the three landscape compartments: colluvial deposits at the slope toes of the upland catchments, channel and overbank deposits in the piedmont zone, and the floodplain deposits. (D) Kernel density estimates of the radiocarbon ages obtained from the three landscape compartments as a measure of residence time of the sediments within them. The grey lines represent kernel density estimates of bootstrapped samples from all samples in the respective compartment; the step-like line represents the number of sequences covering the respective time period. (E) Sketch of a cascading system along a topographic gradient from the hillslopes of the headwater catchments to the floodplain of the receiving stream (SD = slope deposits; CD = colluvial deposits; COD = channel bed and overbank deposits). [Colour figure can be viewed at wileyonlinelibrary.com]

epochs). Culturally speaking, the PPN in Upper Mesopotamia witnessed the transition from hunter-gatherer to farming communities. Further, cultural key developments, such as sedentism, the process of cultivation and domestication of wild cereals and pulses, and early management and domestication of wild ungulates are locally documented (Peters *et al.*, 1999, 2019; Neef, 2003; Tanno and Willcox, 2006; Clare *et al.*, 2019; Dietrich *et al.*, 2019). In the millennia following the PPN, significant socioeconomic developments occurred – e.g., the introduction of the plough, organized agriculture, and the seeder plough (Potts, 1997; Greenfield, 2010; Steadman and McMahon, 2011; Jursa, 2013; Widell *et al.*, 2013) – and the study area continued to hold an important position in the cultural processes of transformation and adaption characterizing ancient Upper Mesopotamia. Accordingly, the environs of Göbekli Tepe provide a unique opportunity to evaluate phases of varying geomorphodynamic activity driven by climatic change and human impact based on the theoretical framework of complex sediment cascades.

We use published (Nykamp *et al.*, 2020a, 2020b) and own unpublished data from sediment sequences to conduct a meta-analysis of varying geomorphodynamic activity by means of cumulative probability functions of radiocarbon ages. The sediment sequences are located in the environs of the hilltop site Göbekli Tepe along a sediment cascade ranging from the slope toes of the headwater catchments across the piedmont zone of the Culap Suyu basin to the floodplain of the Culap Suyu river as the receiving stream. A dataset synopsis (Figure 3) of Holocene climatic (Finné *et al.*, 2019), zooarchaeological (Grupe and Peters, 2011; Peters *et al.*, 2014), demographic (Roberts *et al.*, 2019a), and socioeconomic developments (see Figure 3A for references) points to the potentials and challenges of differentiating complex sediment cascade dynamics and their connection to natural drivers or human impact.

Study Site

The monumental archaeological site of Göbekli Tepe is located ~12 km northeast of Şanlıurfa in southeastern Anatolia (Figure 1A, B). The present-day climate is semi-arid, with hot and dry summers and wet and mild to cold winters. Heavy rainfall can occur between autumn and early spring (Sörensen, 2007; Kuzucuoğlu *et al.*, 2019). Dwarf scrubland and herb-rich steppes characterize the present-day vegetation on the plateaus, the foothills show an open steppe vegetation with scattered oak and fruit trees, and the plains are intensively used for arable farming made possible by the water of the Atatürk Dam (Rosen, 1997; Özcan *et al.*, 2018; Kuzucuoğlu, 2019; Kuzucuoğlu *et al.*, 2019).

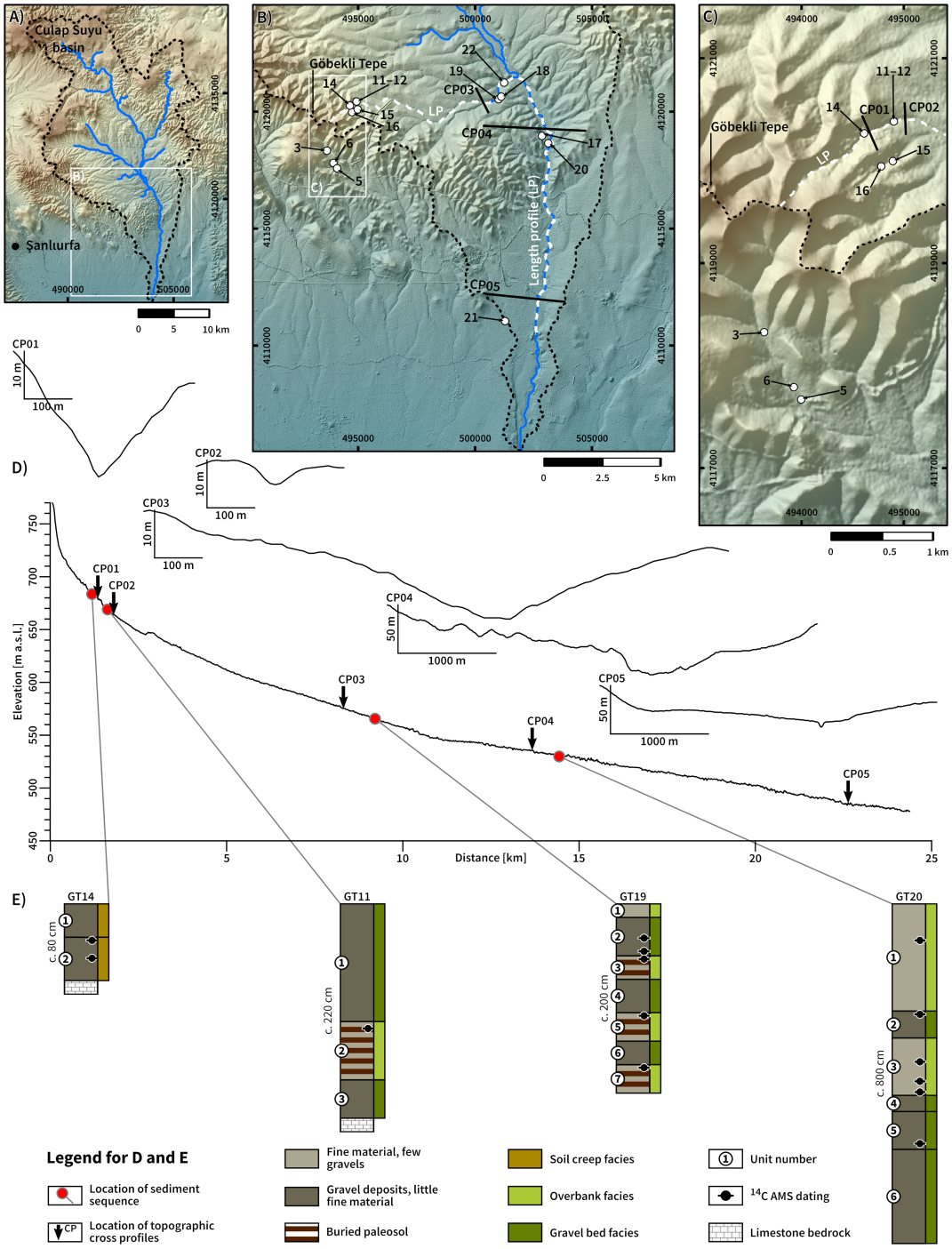

Figure 2. (A) Overview map showing the Culap Suyu basin, its watershed, and drainage network. (B) Map of the lower Culap Suyu basin showing the location of Göbekli Tepe, the locations of the radiocarbon-dated sediment sequences (numbers refer to sequence IDs, cf. Table I) in its vicinity (~12 km max. distance), and the locations of the topographic profiles (length profile = LP; cross profiles 3, 4, and 5 = CP03, CP04, and CP05). (C) Map showing the sediment sequences and topographic profiles (cross-profiles 1 and 2 = CP01 and CP02) that are located in the headwater catchments and the proximal piedmont zone. (D) Topographic length and cross profiles (A–C: spatial reference = WGS84 UTM37N; A–D: height = TanDEM-X elevation data with 12 m × 12 m pixel size, ©DLR 2017). (E) Selected and simplified sediment sequences that are representative for the general conditions in the three landscape compartments. [Colour figure can be viewed at wileyonlinelibrary.com]

The archaeological deposits and architectural remains of Göbekli Tepe rest on a limestone spur of the southern Germuş mountain range, on the southwestern watershed of the Culap Suyu basin, which extends into the wide low-lying Harran plain in the south (Figures 1B and 2A). The flat-lying plateaus consist of different limestone and marl formations of Upper Cretaceous to Lower Miocene age. Locally, remaining patches of Upper Miocene basalt rocks cover the plateaus, forming isolated hills (Geological Research Department, 2014; Kuzucuoğlu *et al.*, 2019). Karstification occurs in areas that are dominated by chalky limestones, whereas clayey limestones show little karstic features. Surface water can infiltrate and circulate through the cavities of the interlinked fissure systems of the karst massifs and feed springs, e.g., the Urfa-Harran springs (Eroskay, 1982; Elhatip, 1997; Eris and Wittenberg, 2015). Such subsurface drainage systems can substantially reduce surface runoff and related erosion processes (cf. Peng and Wang, 2012). Since the Plio-Pleistocene, combined tectonic, lithological, and climatic effects resulted in valley and floodplain development. The basins (Harran plain and Culap Suyu basin) are filled with Quaternary alluvium derived from reworked soils and slope debris of the surrounding

hillslopes (Wilkinson, 1990; Rosen, 1997; Geological Research Department, 2014; Kuzucuoğlu *et al*., 2019). Expectedly, the thickness of the deposits in the valleys and plains decreases in an upslope direction (Wilkinson, 1990), ranging between ~190–240 cm thickness in the proximal piedmont zone and decreasing to less than 100 cm thickness at the slope toes of the headwater catchments; the upper slopes are usually devoid of sediments (Nykamp *et al*., 2020a). Leptosols, Calcisols, and Cambisols have developed in the carbonate-rich parent material of the plateaus and slopes. The plains are characterized by Vertisols (Özcan *et al*., 2018; Akça *et al*., 2018a, 2018b). Recently published results regarding present-day landform characteristics (Knitter *et al*., 2019) and Holocene relief-forming processes (Nykamp *et al*., 2020a) show that the hillslopes of the headwater catchments are characterized by periodic sheet flow and soil creep processes, forming colluvial deposits at the slope toes of the valleys. Episodic torrential rains cause concentrated runoff along the thalwegs of the confined valleys in the headwater catchments, leading to erosion of the colluvial deposits. The entrained sediments are transported out of the valleys, forming channel bed and overbank deposits in the adjacent piedmont zone. Phases of reduced geomorphodynamic activity are documented by topsoil horizons that formed in situ in the overbank deposits of the proximal piedmont zone. Phases of reinforced geomorphodynamic activity during the Bronze Age led to their burial by channel bed and overbank sediments (Nykamp *et al*., 2020a, 2020b).

Material and Methods

During two field campaigns, geomorphological mapping was carried out and sediment sequences were recorded from outcrops and corings. All sediments were described in the field and sampled for subsequent sediment analyses and radiocarbon dating (for details see Nykamp *et al*., 2020a, 2020b). Our sediment records are located within the three major landscape compartments: (1) the upland; (2) the piedmont zone; and (3) the floodplain of the receiving stream (Figure 1C), in the close vicinity (~12 km max. distance) of Göbekli Tepe. For the upland and the proximal part of the piedmont zone, results on sediment architecture, geochemical properties, and chronology are presented by Nykamp *et al*. (2020a, 2020b). For the distal part of the piedmont zone and the floodplain of the receiving stream, sediment analyses are yet not finished. In this study we focus on the radiocarbon chronology and include preliminary findings from field descriptions.

The three studied landscape compartments form a nested hierarchy of interlinked subsystems (*sensu* Chorley and Kennedy, 1971; cf. Figure 1C for visualization). The connectivity within (e.g., within-hillslope) and among them (e.g., hillslope-to-channel; cf. Figure 1E for visualization) occurs at local and regional scales (*sensu* Fryirs *et al*., 2007). The transfer of sediments on all three scales is a function of magnitude–frequency characteristics of external forces, geomorphological thresholds, and time (cf. Chorley and Kennedy, 1971; Schumm, 1973). Each compartment is characterized by a set of parameters – e.g., slope, valley confinement, and sediment texture – that influence surface processes and lead to the development or reworking of landforms (cf. Brierley *et al*., 2006). The durability of the studied landforms and the residence times of the sediments stored within them differ considerably (Figure 1D; cf. Harvey, 2002).

The presented chronological dataset from the surroundings of Göbekli Tepe totals 42 ^{14}C ages that were obtained from 14 sediment sequences (Table I; Figures 1B and 2B, C). We used charcoal pieces and bulk samples containing organic matter from buried organic-rich topsoil horizons or reworked soil sediments for radiocarbon dating. Compared to other studies using cumulative probability functions as a proxy for phases of varying geomorphodynamic activity, we use a rather small number of radiocarbon ages. Therefore, a differentiation among the different archives or a subdivision into 'activity' and 'stability' ages (e.g., Hoffmann *et al*., 2008) is not meaningful. We interpret the radiocarbon ages from charcoal as maximum deposition ages since reworking cannot be excluded (Lang and Hönscheidt, 1999; Chiverrell et al., 2007). Radiocarbon ages obtained from organic matter of buried topsoil horizons are interpreted as maximum age estimates for the time of burial (Scharpenseel and Schiffmann, 1977). Radiocarbon ages achieved from organic matter of buried reworked soil sediments reflect the termination of fresh carbon input into the sediment layer (Dreibrodt *et al*., 2013), but also include allochthonous material (Scharpenseel and Schiffmann, 1977).

The formal subdivision of the Holocene is based on Walker *et al*. (2019) and the boundary between the Younger Dryas and the Early Holocene is set to 11.7 ka BP according to Roberts *et al*. (2018).

For each sediment sequence, depth, and radiocarbon age of the dated samples, the total thickness of the sequence and the landscape compartment (Tables I and II) are recorded. All radiocarbon ages were calibrated using the rcarbon package

Table I. Detailed information on the presented sediment sequences

Sequence ID	UTM 37 N		Elevation (m a.s.l.)	Thickness (cm b.g.s.)	Contributing area (km^2)	Landscape compartment	Extraction method
	Easting	Northing					
GT03	493 656	4 118 322	661.4	74	0.003	Slope toe	Outcrop
GT16	494 800	4 119 940	682.7	78	0.005	Slope toe	Outcrop
GT15	494 912	4 119 993	679.9	60	0.006	Slope toe	Outcrop
GT14	494 632	4 120 264	682.8	80	0.021	Slope toe	Outcrop
GT11	494 922	4 120 378	670.9	224	0.523	Piedmont zone	Outcrop
GT12	494 925	4 120 380	670.9	240	0.523	Piedmont zone	Outcrop
GT06	493 946	4 117 785	641.3	238	1.962	Piedmont zone	Outcrop
GT05	494 017	4 117 664	638.3	192	2.026	Piedmont zone	Outcrop
GT18	501 015	4 120 596	565.9	600	14.55	Piedmont zone	Coring
GT19	500 973	4 120 569	566.5	200	14.55	Piedmont zone	Outcrop
GT22	501 202	4 121 326	557.0	655	21.64	Piedmont zone	Coring
GT17	502 949	4 118 940	534.2	679	434.9	Floodplain	Coring
GT20	503 214	4 118 629	530.8	800	436.2	Floodplain	Coring
GT21	501 326	4 111 007	490.5	530	481.7	Floodplain	Coring

Table II. Results of the radiocarbon datings and their calibration

Sample ID	Lab. ID	Mat.	^{14}C age	Uncertainty (±)	cal. BP (before 1950; 2σ)	cal. BCE/CE (2σ)	Landscape compartment	Ref.
GT03 59-61	POZ-109741	OM	3 290 BP	40	3 613 to 3 408	−1 664 to −1 459	Slope toe	1
GT05 90-92	POZ-109743	OM	2 170 BP	35	2 310 to 2062	−361 to −113	Slope toe	1
GT05 120-122	POZ-109744	OM	1760 BP	30	1 780 to 1 567	171 to 383	Piedmont zone	1
GT06 105-108	POZ-109745	OM	3 400 BP	50	3 828 to 3 509	−1879 to −1 560	Piedmont zone	1
GT11 125-130	TÜBİTAK-0315	OM	3 808 BP	32	4 349 to 4 088	−2 400 to −2 139	Piedmont zone	1
GT12 167-172	TÜBİTAK-0316	OM	4 222 BP	32	4 856 to 4 643	−2 907 to −2 694	Piedmont zone	1
GT14 37-42	POZ-109747	OM	625 BP	30	661 to 551	1 290 to 1 399	Slope toe	1
GT15 29-34	POZ-109749	OM	1 130 BP	30	1 173 to 962	777 to 988	Slope toe	1
GT16 61-65	POZ-109750	OM	1 795 BP	30	1819 to 1 623	132 to 328	Slope toe	1
GT17 205-213	TÜBİTAK-0508	C	4 217 BP	29	4 853 to 4 645	−2 904 to −2 696	Floodplain	2
GT17 250	TÜBİTAK-0509	C	6 158 BP	42	7 169 to 6 941	−5 220 to −4 992	Floodplain	2
GT17 367-370	TÜBİTAK-0510	OM	11 425 BP	44	13 379 to 13 145	−11 430 to −11 196	Floodplain	2
GT17 431	TÜBİTAK-0511	C	11 700 BP	50	13 705 to 13 423	−11 756 to −11 474	Floodplain	2
GT18 134	TÜBİTAK-0512	C	3 668 BP	35	4 090 to 3 894	−2 141 to −1 945	Piedmont zone	2
GT18 168	TÜBİTAK-0513	C	5 977 BP	42	6 935 to 6 694	−4 986 to −4 745	Piedmont zone	2
GT18 183-185	TÜBİTAK-0514	OM	3 780 BP	31	4 247 to 4 006	−2 298 to −2 057	Piedmont zone	2
GT18 290-292	TÜBİTAK-0515	C	4 941 BP	30	5 727 to 5 603	−3 778 to −3 654	Piedmont zone	2
GT18 320-322	TÜBİTAK-0516	OM	4 626 BP	30	5 462 to 5 300	−3 513 to −3 351	Piedmont zone	2
GT18 327-328	TÜBİTAK-0517	C	6 499 BP	33	7 473 to 7 324	−5 524 to −5 375	Piedmont zone	2
GT18 553-554	TÜBİTAK-0518	C	7 763 BP	37	8 603 to 8 444	−6 654 to −6 495	Piedmont zone	2
GT19 35	TÜBİTAK-0519	C	1 648 BP	34	1 688 to 1 416	263 to 535	Piedmont zone	2
GT19 51	TÜBİTAK-0520	C	3 416 BP	28	3 817 to 3 581	−1 868 to −1 632	Piedmont zone	2
GT19 56-58	TÜBİTAK-0521	OM	3 264 BP	28	3 565 to 3 408	−1 616 to −1 459	Piedmont zone	2
GT19 117-119	TÜBİTAK-0522	OM	4 307 BP	29	4 960 to 4 833	−3 011 to −2 884	Piedmont zone	2
GT19 170-172	TÜBİTAK-0523	OM	8 160 BP	37	9 253 to 9 011	−7 304 to −7 062	Piedmont zone	2
GT20 82-85	TÜBİTAK-0524	C	1 687 BP	29	1 693 to 1 534	257 to 417	Floodplain	2
GT20 249	TÜBİTAK-0525	C	3 571 BP	43	3 981 to 3 721	−2 032 to −1 772	Floodplain	2
GT20 375	TÜBİTAK-0526	C	4 074 BP	32	4 806 to 4 440	−2 857 to −2 491	Floodplain	2
GT20 419-422	Poz-110,446	C	4 130 BP	50	4 826 to 4 526	−2 877 to −2 577	Floodplain	2
GT20 446-449	TÜBİTAK-0527	C	6 068 BP	32	7 006 to 6 799	−5 057 to −4 850	Floodplain	2
GT20 564-568	TÜBİTAK-0528	C	9 772 BP	52	11 269 to 11 099	−9 320 to −9 150	Floodplain	2
GT21 164-171	TÜBİTAK-0529	C	10 098 BP	41	11 963 to 11 404	−10 014 to −9 455	Floodplain	2
GT21 190-197	TÜBİTAK-0530	C	13 873 BP	52	17 030 to 16 552	−15 081 to −14 603	Floodplain	2
GT21 332-334	TÜBİTAK-0531	C	17 170 BP	63	20 925 to 20 515	−18 976 to −18 566	Floodplain	2
GT22 87-88	TÜBİTAK-0532	C	3 216 BP	28	3 547 to 3 374	−1 598 to −1 425	Piedmont zone	2
GT22 168		C	6 712 BP	42	7 661 to 7 507	−5 712 to −5 558	Piedmont zone	2

(*Continues*)

Table II. (Continued)

Sample ID	Lab. ID	Mat.	^{14}C age	Uncertainty (±)	cal. BP (before 1950; 2σ)	cal. BCE/CE (2σ)	Landscape compartment	Ref.
	TÜBİTAK-0533							
GT22 208	TÜBİTAK-0534	C	4 669 BP	39	5 575 to 5 312	−3 626 to −3 363	Piedmont zone	2
GT22 279	TÜBİTAK-0535	C	4 764 BP	31	5 589 to 5 333	−3 640 to −3 384	Piedmont zone	2
GT22 341-343	Poz-110,500	C	4 730 BP	40	5 585 to 5 325	−3 636 to −3 376	Piedmont zone	2
GT22 375	TÜBİTAK-0536	C	8 310 BP	36	9 444 to 9 143	−7 495 to −7 194	Piedmont zone	2
GT22 472-474	TÜBİTAK-0537	C	13 730 BP	56	16 850 to 16 330	−14 901 to −14 381	Piedmont zone	2
GT22 547	TÜBİTAK-0538	C	14 612 BP	66	17 985 to 17 595	−16 036 to −15 646	Piedmont zone	2

Sample ID = combination of sediment sequence ID and sample depth in cm b.g.s.; Mat. = dated material; OM = bulk samples containing organic matter; C = charcoal; Ref. = reference; 1 = Nykamp *et al.* (2020a); 2 = this study.

(Bevan and Crema, 2018) and the IntCal13 calibration curve (Reimer *et al.*, 2013). We calculated a cumulative probability function (CPF; spd function, rcarbon package; raw data and R code: Supporting Information S1–S4) of all ^{14}C ages assuming that the cumulative likelihood is proportional to phases of intensified geomorphodynamic activity reflected in the sediment sequences (e.g., Chiverrell *et al.*, 2011). The CPF was normalized to unity and smoothed with a moving window (size 1000) to avoid a dominance of peaks caused by single isolated dates.

The relationship between age probability and phases of intensified geomorphodynamic activity is not straightforward and biased; e.g., steeper parts of the calibration curve result in artificial peaks in the CPF (Hoffmann *et al.*, 2008; Carleton and Groucutt, 2019). Periods of enhanced fire activity result in an increased availability of datable material, leading to increased cumulative probability, although not directly linked to phases of intensified sediment dynamics (Carleton and Groucutt, 2019). Furthermore, radiocarbon dates from sediment sequences are not necessarily related to depositional events, but can be reworked and redeposited (e.g., Chiverrell *et al.*, 2011). Consequently, the sample size of all available radiocarbon ages is crucial, because single dates can have an important influence on a CPF. Regarding palaeoenvironmental archives, a major issue is a preservation bias. Reworking and incompleteness of the record grows with increasing time difference between sampling and sedimentation (Lewin and Macklin, 2003; Macklin *et al.*, 2005; cf. Williams, 2012; Carleton and Groucutt, 2019). To consider these biases, we tested our observed CPF against simulated CPFs (cf. also Becker *et al.*, 2020).

Simulated CPFs were calculated from simulated random radiocarbon ages over the time period covered by the observed CPF. The probability that an age is sampled and used during a simulation run is equal to the probability that the age is covered by the available sediment sequences. Therefore, a potential maximum age of each sediment sequence is estimated as a function of the sedimentation rate, which is given by each radiocarbon age and the depth from which the sample was obtained (cf. Dusar *et al.*, 2012). The estimated maximum age covered by a sequence is assumed to be a function of the sequences' thickness and the median of all sedimentation rates of a sequence. The number of samples in each simulation run is equal to the given number of ages. This allows for a robust estimate of the variability given by the number of observed ages. As the simulated CPFs and the observed CPF are both subject to the variability of the calibration curve, we did not standardize the observed CPF by dividing it by the calibration curve (cf. Hoffmann *et al.*, 2008). Random ages were back-calibrated to acquire uncalibrated radiocarbon ages of a randomly sampled age (uncalibrate function, rcarbon package). Thereafter, these radiocarbon ages were calibrated to calculate the CPFs. The error of each back-calibrated age is estimated based on a linear model of the observed ^{14}C ages and their errors. We calculated 1000 different simulated CPFs.

Calculating the difference between the observed CPF and each simulated CPF allows us to assess the likelihood of the observed CPF being higher than the simulated CPFs. The proportion of cases where a peak of the observed CPF is greater than the respective part of a simulated CPF is assumed to be equal to the likelihood that this peak of the observed CPF is not random.

In addition to the observed CPF of all ages, we calculated Gaussian kernel density estimates using a window of 1000 years (Supporting Information S2, S3). We interpret the number of sequences covering a defined time period and their age density as an indicator for the residence time of sediments in the archives.

Results

The upland (Figure 1C) comprises low-order catchments characterized by narrow valleys with steep hillslopes and thalwegs showing strongly concave length profiles (cf. LP and CP01 in Figure 2D). The hillslopes of these headwater areas are usually characterized by frequently outcropping bedrock and locally occurring thin sediment covers. At the slope toes of the upland catchments often colluvial deposits are formed (Figure 1E). The colluvial deposits have short residence times (Figure 1D) and the slope toes form transient landforms.

The strong flow convergence within these steep and confined valleys (cf. LP and CP01 in Figure 2D) allows concentrated overland flow occurring after precipitation events of sufficient intensity that erodes the colluvial deposits along the thalwegs. At the transition between the upland and the piedmont zone, the confinement and inclination of the valleys decrease (cf. LP and CP02 in Figure 2D), and the reworked colluvial sediments are deposited in channel bed and overbank settings (Figure 1E). Phases of geomorphodynamic stability during the Holocene are documented by palaeosols that were buried by gravel bed or overbank deposits during subsequent

phases of geomorphodynamic activity (cf. GT11 and GT19 in Figure 2E).

The contributing area at the locations where the sediment sequences were extracted increases substantially from a few thousand square metres at the slope toes (0.003–0.021 km^2) to several square kilometres in the piedmont zone (0.523–21.64 km^2; Table I). Locally, the deposits in the piedmont zone are eroded by fluvial dynamics along the channels of the tributaries and transported downstream to lower compartments of the cascade (Figure 1C, E). However, compared to the slope toes, the piedmont zone has a substantial capacity to buffer sediments, as indicated by the increased residence time (Figure 1D). Another abrupt increase in the contributing area at the locations of the sequences occurs after the tributaries enter the floodplain of the receiving stream amounting to several hundred square kilometres (434.9–481.7 km^2; Table I). The floodplain is characterized by a rather straight and gently sloping length profile section compared to the sections that run through the piedmont zone and the upland showing increasing inclination and concavities in upslope direction (cf. LP in Figure 2D). The floodplain sediments of the Culap Suyu river are characterized by alternating layers of gravel deposits related to channel bed dynamics and alluvial loams related to overbank deposition (cf. GT20 in Figure 2E). The residence time of these sediments is considerably longer than in the other compartments (Figure 1D) due to the low confinement of the valley (cf. CP04 and CP05 in Figure 2D) and the high buffer capacity of the floodplain.

The 42 radiocarbon ages cover the last part of the Late Pleistocene from ~20.5 ka BP and the entire Holocene (Table II). The separate evaluation of the three landscape compartments clearly shows that sediment dynamics in the surroundings of Göbekli Tepe are not equally reflected in each of the different archives: the Late Pleistocene record is mainly preserved in the floodplain, whereas the Early–Middle Holocene record is reflected in the floodplain and piedmont zone, and the Late Holocene record is preserved in all three archives (Figure 1D; Table II).

Our cumulative probability analysis of the radiocarbon ages shows that two main phases of intensified geomorphodynamic activity during the Holocene can be reconstructed for the surroundings of Göbekli Tepe. For both phases the probability of the observed ages is clearly higher than the random variability as expected from simulations. Phase I (ca. 7.4–7.0 ka BP) occurs in the sediment sequences from the piedmont zone and the floodplain. Phase II (ca. 5.8–3.3 ka BP) is represented in the archives from all three compartments. The first phase of intensified geomorphodynamic activity occurred at the transition from the Neolithic to the Chalcolithic and peaked at ca. 7.2 ka BP. The second phase of intensified geomorphodynamic activity (ca. 5.8–3.3 ka BP) occurred during the Late Chalcolithic and the Bronze Age and peaked at ca. 5.1, 4.4, and 3.8 ka BP (Figure 3I).

Discussion

We compare our local CPF with available local to supra-regional datasets of climatic, environmental, and socio-economic change and diachronically discuss cause–effect relationships of possible triggers for phases of intensified geomorphodynamic activity in the surroundings of Göbekli Tepe. We employ *sediment cascades* as a heuristic tool to interpret our fragmentary records. Such a heuristic approach is necessary, because clear causal relationships between phases of intensified geomorphodynamic activity and a certain trigger such as climatic or human impact often cannot be established from alluvial records (cf. Roberts *et al.*, 2019b).

Possible triggers for phases of intensified geomorphodynamic activity in the surroundings of Göbekli Tepe

The curve of the summed probability density (SPD) of ^{14}C dates from archaeological sites in southern Turkey (Figure 3B) shows an initially growing population at around 10.3 ka BP and a peak shortly before 8.0 ka BP. The raw counts of sites from archaeological surveys in southern Turkey indicate a slight increase at around 8.0 ka BP, but mainly reflect the strong population growth starting at the beginning of the Bronze Age around 5.0 ka BP (Roberts *et al.*, 2019a).

The consistency of the standardized hydroclimatic proxy data for the Levant (Figure 3C) and Turkey (Figure 3D) partly varies considerably. The proxy data for the Levant suggest wetter conditions than at present for 10.0–6.1 ka BP and subsequently a generally more arid climate, with two periods of wetter conditions centred at 4.7 and 3.7 ka BP. The proxy data for Turkey show an aridization between 10.0 and 3.0 ka BP, with wetter-than-modern conditions dominating between 10.0 and 4.5 ka BP, and distinct aridity between 3.0 and 1.9 ka BP (Finné *et al.*, 2019).

The $\delta^{18}O$ record from Lake Nar (Figure 3E), central Anatolia, shows dry hydroclimatic conditions for the period of the Younger Dryas and a transition into the relatively wetter Early Holocene (Dean *et al.*, 2015). Also, other regional proxy data consistently suggest highest levels of aridity for the Younger Dryas (ca. 12.5–11.7 ka BP) and a rapid humidity increase at the beginning of the Holocene (Fleitmann *et al.*, 2009; Göktürk *et al.*, 2011; Eriş *et al.*, 2018; Ön *et al.*, 2018; Roberts *et al.*, 2018). Such a large-scale transition from dry to wet conditions should have had an impact on sediment dynamics, as has been suggested for the Eastern Mediterranean (Dusar *et al.*, 2011), but there is no significant increase in our ^{14}C data for this period (Figure 3I). Rather, and in agreement with our observations, Roberts *et al.* (2019b) showed that influx of clastic material into Lake Nar was minimal between ca. 13.8 and 9.3 ka BP despite the major changes in hydroclimate and vegetation associated with the Late Pleistocene–Holocene transition.

Major shifts in subsistence strategies are visible in the considerable and rather sudden reduction of archaeobiodiversity (Shannon entropy) and the synchronous increase of percentage similarity. This trend started towards the end of the 9th millennium BCE and became more pronounced in the first half of the 8th millennium BCE (Peters *et al.*, 2014; Figure 3F). Percentage similarity expresses the similarity of a bone assemblage with that of a typical farming community and confirms the fast shift in subsistence strategies in this region. Human nutrition relied on hunting, fowling, and collecting a broad spectrum of animals during the PPN A and early PPN B. This spectrum became reduced and much more unbalanced in the course of the middle PPN B, with few livestock species clearly dominating the assemblages (Peters *et al.*, 2014).

In Early Holocene settlements located in the wider surroundings of Göbekli Tepe, gazelles dominated the faunal remains until the early PPN B (90% at Göbekli Tepe to 70% at early PPN B Nevali Çori). During the middle PPN B a complete faunal turnover occurred at the advantage of domestic caprines (sheep and goat), accounting for up to 97% of the medium bovid assemblages, illustrating the relatively fast transition from hunting to herding (Peters *et al.*, 2014; Figure 3G).

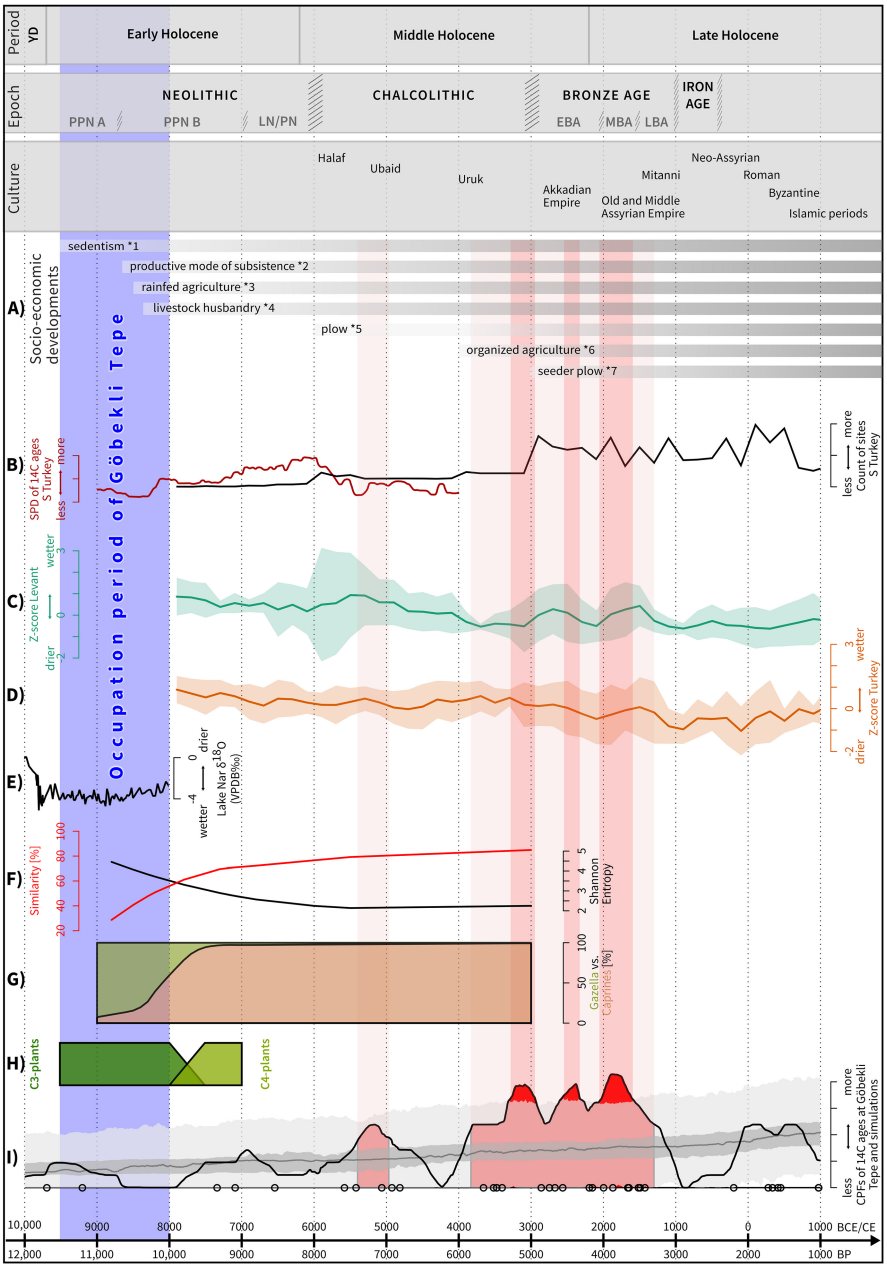

Figure 3. Synoptic illustration of cultural, demographic, climatic, faunal, and vegetational changes during the last 12 000 years in southwestern Asia and the cumulative probability of 42 radiocarbon dates obtained from the vicinity of Göbekli Tepe (transition between Younger Dryas (YD) and Holocene after Roberts *et al.* (2018); subdivision of Holocene according to Walker *et al.* (2019); archaeological chronology according to Anastasio *et al.* (2004); Yardımcı (2004). (A) Societal and cultural key developments and innovations. The periodization of the corresponding cultural epochs and the emergence of socioeconomic developments and innovations is presented in a simplified way. Supra-regional societal and cultural developments and innovations were compared with archaeological finds and evidence for the closer surroundings of Göbekli Tepe. The compilation is based upon: *1 = Clare *et al.* (2019); *2 = Akkermans and Schwartz (2003), Tanno and Willcox (2006), Peters *et al.* (2013, 2014); *3 = Akkermans and Schwartz (2003), Tanno and Willcox (2006), Steadman and McMahon (2011); *4 = Steadman and McMahon (2011), Peters *et al.* (2013), Hammer and Arbuckle (2017); *5 = Greenfield (2010); *6 = Steadman and McMahon (2011); *7 = Potts (1997), Jursa (2013), Widell *et al.* (2013). (B) Demographic trend of Turkey according to the summed probability density (SPD) of ^{14}C dates from archaeological excavations and based on settlement numbers from archaeological site surveys (Roberts *et al.*, 2019a). (C) Regional mean *z*-score and one standard deviation (shaded areas) showing the hydroclimatic variability during the last 10 000 years for the Levant and (D) for Turkey. The *z*-scores were cut off at 10 000 years cal. BP to avoid a possible masking of the more subtle Holocene variability as a consequence of substantial shifts at the Late Pleistocene–Early Holocene transition (Finné *et al.*, 2019). (E) δ^{18}O record from central Anatolian Lake Nar showing a shift from dry to relatively wetter conditions at the Younger Dryas–Holocene transition (Dean *et al.*, 2015). (F) Major changes in human nutrition in southeast Turkey: the archaeobiodiversity index (Shannon entropy) indicates a narrowing of the species spectrum in the meat diet of humans, while percent similarity points to a quick shifting from hunting to herding in the late 9th–early 8th millennium BCE (Peters *et al.*, 2014). (G) Replacement of Persian gazelle by sheep and goat during the second half of the 9th and early 8th millennium BCE at PPN sites, indicating the beginning of caprine pastoralism in southeast Turkey (Peters *et al.*, 2014). (H) Carbon isotope analyses provide evidence for overgrazing of pasture grounds in the vicinity of PPN B settlements. (I) Cumulative probability function (CPF) of 42 radiocarbon dates obtained from the vicinity of Göbekli Tepe (for locations see Figures 1B and 2B, C). The observed CPF (black line) was calculated based on the principles described in Hoffmann *et al.* (2008) and Jones *et al.* (2015), among others, and smoothed using a 1000-year running mean. The grey line and the respective envelope show expected CPFs that were calculated based on Monte Carlo simulations of random samples from a model fitted to the sampling density (estimated number of sequences covering a period: cf. Shennan *et al.*, 2013; Bevan and Crema, 2018; see Supporting Information S2 and S3 for further details); red backgrounds highlight periods with a high likelihood (>83%) that the observed CPF exceeds the expected CPFs. [Colour figure can be viewed at wileyonlinelibrary.com]

Carbon isotope analyses revealed a change in the plant diet of humans and animals between the PPN A and late PPN B (Grupe and Peters, 2011; Figure 3H). Wild ungulates, humans and dogs show carbon values typical for a C3 plant diet at Göbekli Tepe and Nevali Çori. At late PPN B Gürcütepe the nutrition of humans and domestic animals contained significantly more C4 plants, while the wild animals apparently continued exploiting a vegetation cover similar to their wild counterparts in earlier times. This is strong evidence (1) for overgrazing of pasture grounds around the Early Neolithic settlement and (2) that the wild herbivores avoided vegetation cover intensely frequented by domestic livestock (Grupe and Peters, 2011).

Neither the Early Holocene societal, cultural, and land-use changes, such as the emergence of sedentism (Clare *et al.*, 2019), the processing of wild cereals (Dietrich *et al.*, 2019), or the faunal turnover (Peters *et al.*, 2014) causing overgrazing with time (Grupe and Peters, 2011), nor the initial demographic rise around 10.3 ka BP (Roberts *et al.*, 2019a), can be linked to intensified geomorphodynamic activity in the surroundings of Göbekli Tepe (Figure 3A, B, F–I). This might be due to an extensive erosional phase that has caused an erosion discontinuity in the sediment records from the northern Harran plain and the proximal piedmont zone of the Culap Suyu basin (Rosen, 1997; Nykamp *et al.*, 2020a). However, while the results of Rosen (1997) suggest that this phase occurred during the Late Pleistocene, the results of Nykamp *et al.* (2020a) now suggest an Early–Middle Holocene timing.

The first phase of intensified geomorphodynamic activity around Göbekli Tepe (ca. 7.4–7.0 ka BP; Figure 3I) followed the population growth that occurred around 8.0 ka BP (Figure 3B; Roberts *et al.*, 2019a). Accompanying sociocultural developments and land-use change may also have contributed to intensified geomorphodynamic activity, as animal husbandry (Steadman and McMahon, 2011; Peters *et al.*, 2013; Hammer and Arbuckle, 2017), rainfed agriculture (Akkermans and Schwartz, 2003; Tanno and Willcox, 2006; Steadman and McMahon, 2011), and the use of the plough (Greenfield, 2010), for example, were already well established (Figure 3A). Such agricultural activities often cause intensified geomorphodynamic activity (Fuchs and Zöller, 2006; Dreibrodt *et al.*, 2010; Notebaert *et al.*, 2011; Houben *et al.*, 2012). Thus human impact can be assumed to represent one of the main driving forces for this phase of intensified geomorphodynamic activity. Climatically, this period was characterized by generally wetter-than-modern conditions in the Levant and Turkey. However, aridization occurred in Turkey after ca. 7.3 ka BP (Figure 3D; Finné *et al.*, 2019) and, therefore, a climatic impact on the intensified geomorphodynamic activity cannot be excluded.

The second phase of intensified geomorphodynamic activity (ca. 5.8–3.3 ka BP; Figure 3I) occurred simultaneously with a phase of substantially increased sediment dynamics in the entire Eastern Mediterranean region as a consequence of widespread increased human impact (Dusar *et al.*, 2011). During this period several innovations and new land-use techniques occurred (Figure 3A), such as the emergence of organized agriculture (Steadman and McMahon, 2011) and the use of the seeder plough (Potts, 1997; Jursa, 2013; Widell *et al.*, 2013). Climatically, this period coincided with the final stage of aridization in Turkey, with drier conditions than present day after ca. 4.5 ka BP, and generally more arid conditions in the Levant after ca. 6.1 ka BP (Figure 3C, D; Finné *et al.*, 2019). This phase of intensified geomorphodynamic activity peaked at 5.1, 4.4, and 3.8 ka BP.

The first peak of intensified geomorphodynamic activity at ca. 5.1 ka BP preceded the substantial population growth at the Chalcolithic–Bronze Age transition by about 100 years (cf. Figure 3B, I; Roberts *et al.*, 2019a) and is recorded in the sediments of the piedmont zone and floodplain (Figure 1D). This temporal gap may result from the resolution of our CPF – CPFs are usually not able to record short events – or the storage of sediments in temporal sinks that were not captured by our dataset. The second peak of intensified geomorphodynamic activity at ca. 4.4 ka BP was recorded in the piedmont zone and floodplain sequences and occurred after the Bronze Age population growth after 5.0 ka BP. However, both hydroclimatic proxy datasets consistently show a substantial aridization between 4.7 and 4.1 ka BP coinciding with this second peak. The third peak of intensified geomorphodynamic activity at ca. 3.8 ka BP coincided with increasingly humid conditions in Turkey and the Levant between 4.1 and 3.5 ka BP (Figure 3B, C, I; Finné *et al.*, 2019). Mainly the sediments in the piedmont zone and floodplain, and to a lesser degree the sequences from the upland, provide records for this peak (Figure 1D).

At the time when the intensified geomorphodynamic activity peaked at ca. 4.4 and 3.8 ka BP, conditions prevailed that often correlate with geomorphological instability in semi-arid environments (cf. Walsh *et al.*, 2019), whereby the increasing and lasting land-use pressure during the Bronze Age intensified the effects of aridization on geomorphodynamic activity between 4.7 and 4.1 ka BP. Aridization caused degradation of the vegetation cover and resulted in amplified landscape sensitivity to the increasing frequency of torrential rain events. As a consequence of the degraded vegetation cover, the ongoing exploitation of cultural landscapes presumably fostered soil erosion during the return to wetter conditions between 4.1 and 3.5 ka BP. Finally, in our dataset, the phase of pronounced aridity in Turkey between 3.0 and 1.9 ka BP (Finné *et al.*, 2019) shows a complete lack of ^{14}C dates (cf. Figure 3D, I).

Phases of intensified geomorphodynamic activity along the sediment cascade

Generally, the connectivity of sediments along a sediment cascade depends on the presence and character of landform impediments, i.e. buffers, barriers, and blankets. Buffers include landforms such as alluvial fans, piedmont zones or low slope alluvial floodplains disrupting lateral and longitudinal linkages within a catchment (Fryirs *et al.*, 2007). The deposits stored within these buffers are used to study the palaeoenvironmental evolution in relation to, for example, large-scale climate forcing (e.g., Hoffmann *et al.*, 2008; Wolf and Faust, 2015; Faust and Wolf, 2017) or the extent of past local to regional human impact (e.g., Lang and Hönscheidt, 1999; Chiverrell *et al.*, 2007; Hoffmann *et al.*, 2008; Fuchs *et al.*, 2011; Houben *et al.*, 2012). Thus the inherent characteristics of buffers, their locations within the catchment, and the varying residence times of sediments in these storage units (Fryirs *et al.*, 2007; Fryirs, 2013) are directly linked to peculiarities of the respective archives. As stated by Lewin and Macklin (2003), floodplain archives are more likely controlled by climate than by human impact, or rather store regional trends of land-use change (cf. Dotterweich, 2008). Archives that more directly reflect human impact are often found in first-order catchments (Fuchs and Zöller, 2006; Dotterweich, 2008), but these archives are usually characterized by comparably low residence times (Harvey, 2002).

The varying preservation conditions among the different compartments are a consequence of the markedly different magnitude–frequency characteristics of perturbations – e.g.,

rainstorm events, controlling sediment transport events on slopes and in rivers (cf. Bracken et al., 2015) – and have important implications for the understanding of early human impact. In the surroundings of Göbekli Tepe, radiocarbon ages obtained from colluvial deposits from the slope toes of the headwater catchments only cover the Late Holocene, while the Late Pleistocene until the Late Holocene is recorded in the floodplain deposits of the Culap Suyu river (Figure 1D).

The tendency of observing younger sediments in the upland and older sediments predominantly in the piedmont zone and floodplain (Figure 1C) is not necessarily in accordance with literature that relates sediment dynamics and human occupation. Fuchs *et al*. (2011) observed colluvial sediment sequences related to Neolithic farming, which clearly pre-date sediments from alluvial archives. Also, Fuchs and Zöller (2006), Dreibrodt *et al*. (2010), Notebaert *et al*. (2011), and Houben *et al*. (2012) observed similar age–archive relations (cf. also Lewin and Macklin, 2003; Keen-Zebert *et al*., 2013). In all these studies early agriculture was reflected in those archives that were most directly linked to human activities, i.e. colluvial deposits (Fuchs *et al*., 2004). This is not the case for the environs of Göbekli Tepe.

We argue that poor preservation is one reason for the lacking colluvial deposits that might have provided signals of early human impact during the PPN at Göbekli Tepe. Here Neolithic human impact started much earlier than in Europe; thus possible colluvial deposits were longer exposed to erosion (cf. Zolitschka *et al*., 2003) – e.g., during the Bronze Age, when regional sediment dynamics increased dramatically (Dusar *et al*., 2011). Another reason for the lack of PPN colluvial deposits can also be the relatively low human impact during the Early Holocene compared to later Holocene periods and the generally low landscape sensitivity to erosion during this time (Dusar *et al*., 2011). This, however, cannot explain the observed lack of colluvial deposits from the Chalcolithic or Early Bronze Age. Therefore, we assume that the colluvial deposits in a semi-arid system such as the Culap Suyu basin more likely reflect the time since the last high magnitude–low frequency event that was effective enough to flush the sediments through the system (cf. Fryirs *et al*., 2007, and references therein).

Limitations for the identification of clear cause–effect relationships

Our synoptic illustration of local, regional and supra-regional datasets allows a diachronic comparison and the identification of possible triggers of intensified geomorphodynamic activity (Figure 3). This helps to disentangle natural drivers and effects of human impact, but also shows the limitations of this approach. These limitations include the availability and spatial scales of the datasets that are compared with our local CPF, our local CPF dataset itself, and the interpretation of cause–effect relationships of possible key driving forces that might have provoked intensified geomorphodynamic activity.

While some datasets allow us to reconstruct certain developments on local to regional scales – e.g., evidence for sedentism (Clare *et al*., 2019), for the processing of wild cereals (Dietrich *et al*., 2019), or for the fast shift in subsistence strategies from hunting to herding (Peters *et al*., 2014), and overgrazing of pasture grounds (Grupe and Peters, 2011) – other datasets are only available on regional to supra-regional scales. The demographic trends for southern Turkey (Roberts *et al*., 2019a) can be considered as regional and the hydroclimatic proxy data for Turkey and the Levant (Finné *et al*., 2019) as supra-regional. Such a lack of local diachronic datasets undoubtedly increases the uncertainty identifying possible triggers of intensified geomorphodynamic activity.

Our observed CPF of 42 radiocarbon ages from the vicinity of Göbekli Tepe and its interpretation also face various difficulties and weaknesses, i.e. the relatively small sample size and potential redeposition of the sampled material (see 'Material and Methods', above). However, we argue that our data reflect the general trend of intensified and reduced geomorphodynamic activity. On the one hand, we averaged the CPF using a running mean of 1000 years. This operation reduces the sensitivity of the CPF to repositioning of dated samples and age inversions, which occur in GT05, GT18, GT19, and GT22 (Table II). Thus it ensures that the peaks in the CPF are less likely based only on a single radiocarbon age. Additionally, the residence time in different archives is accounted for by simulating the average period covered by the sediment sequences. On the other hand, our interpretations are based on those phases and peaks in the CPF that clearly exceed CPFs of simulated ^{14}C ages that are equally distributed over the available sediment sequences (Monte Carlo simulations). As the number of ages in each simulation run is equal to our relatively small number of observed radiocarbon ages, the effect of sample size is taken into account by the test. This in turn reduces the risk of overinterpretation of peaks that are based on a small number of ^{14}C ages.

The establishment of clear cause–effect relationships between phases of intensified geomorphodynamic activity and climatic or anthropogenic impacts represents another difficulty. It can be problematic unless sediment archives such as varved sediment sequences from endorheic lake basins with small catchment areas are studied. Roberts *et al*. (2019b) investigated such sediments from the central Anatolian Lake Nar, a maar lake with a diameter of ~0.5 km and a catchment area of ~4 km^2 (including lake surface). They conclude that deforestation, cereal and tree crop cultivation, and livestock grazing were the primary causes for Late Holocene badland expansion in Cappadocia. Besides, climate change, notably during dry–wet or wet–dry transitional phases, may have acted synergistically on erosion acceleration (Roberts *et al*., 2019b). Conclusions obtained from such a narrowly confined lake system cannot be achieved from alluvial sediment archives at catchment scale having dimensions like the Culap Suyu basin.

Nonlinear responses of the geomorphological system to climatic and anthropogenic triggers, its system-inherent complexity and internal feedback mechanisms, and the complex interdependencies among them often complicate the identification of clear cause–effect relationships (Verstraeten *et al*., 2017). Further, the climatic and anthropogenic triggers are often interacting; one signal might level or accelerate another signal (cf. Bintliff, 2002; Fuchs, 2007). Thus, as also shown in this study, the complex dynamic nature of a given geomorphodynamic system often prohibits to directly link natural or anthropogenic events and changes to sedimentary signals in alluvial sequences. From this perspective, an integrative and complementary setup of empirical and theoretical models is a prerequisite in order to disentangle the investigated archives and to gain more profound insights into the development of human–environment interactions.

Conclusions

The presented cumulative probability function of ^{14}C dates from sediment sequences obtained from the environs of Göbekli Tepe is in good agreement with the general trend of increased sediment dynamics in the Eastern Mediterranean.

The observed phases of intensified geomorphodynamic activity at ca. 7.4–7.0 and 5.8–3.3 ka BP roughly correspond to phases of demographic, socioeconomic, and climatic dynamics. The phase of intensified geomorphodynamic activity at ca. 7.4–7.0 followed the population growth at ca. 8.0 ka BP and already established land use practices such as rainfed agriculture or ploughing, and also coincided with aridization in Turkey after ca. 7.3 ka BP. The phase of intensified geomorphodynamic activity at ca. 5.8–3.3 ka BP coincided with demographic and socioeconomic developments such as the major Bronze Age population growth at ca. 5.1 ka BP and the emergence of organized agriculture as well as with the final stage of mid-Holocene aridization in Turkey. Even though these phases partially coincided quite well with possible triggers, the derivation of clear cause–effect relationships is not straightforward. Unlike both mid-Holocene phases of intensified geomorphodynamic activity, neither the extensive climatic change at the Younger Dryas–Holocene transition, nor the introduction of herding in the vicinity of Göbekli Tepe left a clear signature in our dataset. The separate evaluation of the deposits from the different hierarchical landscape compartments provides a detailed insight into the spatiotemporal coverage of these sediment archives. Phases of varying geomorphodynamic activity are not equally reflected in the archives; this especially holds true for the colluvial deposits in the upland. Presumably, these archives would be particularly suitable in studying early Neolithic human impacts at the hilltop site Göbekli Tepe as they are highly sensitive and directly linked to human activities, but they only cover the Late Holocene. Thus, in semi-arid environments, the preservation of these deposits represents a key requirement when studying ancient hilltop sites such as Göbekli Tepe. Besides, the nonlinear relationships governing complex geomorphological and sociocultural phenomena should be elucidated in far more detail, conceivably a challenging task for future studies.

Acknowledgements—We thank the German Research Foundation (Deutsche Forschungsgemeinschaft, DFG) for funding this project (SCHU 949/15-3; PE 424/10-1,4) and the General Directorate of Cultural Assets and Museums, Ministry of Culture and Tourism of Turkey and the Şanlıurfa Museum for making research possible. RB and DK also thank the Collaborative Research Center 1266 'Scales of Transformation' (Deutsche Forschungsgemeinschaft, DFG, project number 2901391021). We acknowledge support by the Open Access Publication Fund of Freie Universität Berlin. Martin Finné is acknowledged for kindly providing the hydroclimatic z-scores for Turkey and the Levant. We thank Max Engel and two anonymous reviewers for thoroughly evaluating our manuscript; their valuable comments and suggestions considerably improved earlier versions of this manuscript. We also thank Editor-in-Chief Stuart Lane and Special Edition Editor Julia Meister for handling and evaluating our manuscript. Open access funding enabled and organized by Projekt DEAL.

Conflict of Interest

The authors declare no conflict of interest.

Data Availability Statement

The data that support the findings of this study are available in the supplementary material of this article or from the corresponding author upon request.

References

Akça E, Aydemir S, Kadir S, Eren M, Zucca C, Günal H, Previtali F, Zdruli P, Çilek A, Budak M, Karakeçe A, Kapur S, FitzPatrick AE. 2018a. Calcisols and Leptosols. In *The Soils of Turkey*, Kapur S, Akça E, Günal H (eds). Springer: Cham, Switzerland; 139–167.

Akça E, Polat S, Razzaghi S, Vignozzi N, Kaya Z, Kapur S. 2018b. Cambisols and Leptosols. In *The Soils of Turkey*, Kapur S, Akça E, Günal H (eds). Springer: Cham, Switzerland; 111–128.

Akkermans PMMG, Schwartz GM. 2003. *The Archaeology of Syria: From Complex Hunter-Gatherers to Early Urban Societies (ca.16000–300 BC)*. Cambridge University Press: Cambridge, UK.

Anastasio S, Lebeau M, Sauvage M, Pruss A. 2004. *Atlas of Preclassical Upper Mesopotamia (APUM)*, Subartu 13. Brepols: Turnhout, Belgium.

Becker F, Knitter D, Nykamp M, Schütt B. 2020. Meta-analysis of geomorphodynamics in the Western Lower Bakırçay Plain (Aegean Region, Turkey). *Land* **9**(9): 1–29.

Bevan A, Crema ER. 2018. rcarbon v1.2.0: Methods for calibrating and analysing radiocarbon dates. Available: https://CRAN.R-project.org/package=rcarbon [26 March 2020].

Bintliff J. 2002. Time, process and catastrophism in the study of Mediterranean alluvial history: a review. *World Archaeology* **33**(3): 417–435.

Bracken LJ, Turnbull L, Wainwright J, Bogaart P. 2015. Sediment connectivity: a framework for understanding sediment transfer at multiple scales. *Earth Surface Processes and Landforms* **40**: 177–188.

Brierley G, Fryirs K, Jain V. 2006. Landscape connectivity: the geographic basis of geomorphic applications. *Area* **38**(2): 165–174.

Carleton WC, Groucutt H. 2019. Sum things are not what they seem: problems with the interpretation and analysis of radiocarbon-date proxies. *SocArXiv preprint server*. https://doi.org/10.31235/osf.io/yp38j

Chiverrell RC, Harvey AM, Foster GC. 2007. Hillslope gullying in the Solway Firth–Morecambe Bay region Great Britain: responses to human impact and/or climatic deterioration? *Geomorphology* **84**: 317–343.

Chiverrell RC, Thorndycraft VR, Hoffmann TO. 2011. Cumulative probability functions and their role in evaluating the chronology of geomorphological events during the Holocene. *Journal of Quaternary Science* **26**(1): 76–85.

Chorley RJ, Kennedy BA. 1971. *Physical Geography: A Systems approach*. Prentice-Hall: London.

Clare L, Kinzel M, Sönmez D, Uludağ C. 2019. Göbekli Tepe: UNESCO Dünya Miras Alanı ve Değişen Yaklaşımlar. *Mimarlık* **405**: 14–18.

Dean JR, Jones MD, Leng MJ, Noble SR, Metcalfe SE, Sloane HJ, Sahy D, Eastwood WJ. 2015. Eastern Mediterranean hydroclimate over the late glacial and Holocene, reconstructed from the sediments of Nar lake, central Turkey, using stable isotopes and carbonate mineralogy. *Quaternary Science Reviews* **124**: 162–174.

Dietrich L, Meister J, Dietrich O, Notroff J, Kiep J, Heeb J, Beuger A, Schütt B. 2019. Cereal processing at Early Neolithic Göbekli Tepe, southeastern Turkey. *PLoS ONE* **14**(5): 1–34, e0215214.

Dotterweich M. 2008. The history of soil erosion and fluvial deposits in small catchments of central Europe: deciphering the long-term interaction between humans and the environment – a review. *Geomorphology* **101**: 192–208.

Dreibrodt S, Lubos C, Terhorst B, Damm B, Bork H-R. 2010. Historical soil erosion by water in Germany: scales and archives, chronology, research perspectives. *Quaternary International* **222**: 80–95.

Dreibrodt S, Jarecki H, Lubos C, Khamnueva SV, Klamm M, Bork H-R. 2013. Holocene soil formation and soil erosion at a slope beneath the Neolithic earthwork Salzmünde (Saxony-Anhalt, Germany). *Catena* **107**: 1–14.

Dusar B, Verstraeten G, Notebaert B, Bakker J. 2011. Holocene environmental change and its impact on sediment dynamics in the Eastern Mediterranean. *Earth-Science Reviews* **108**: 137–157.

Dusar B, Verstraeten G, D'haen K, Bakker J, Kaptijn E, Waelkens M. 2012. Sensitivity of the Eastern Mediterranean geomorphic system towards environmental change during the Late Holocene: a chronological perspective. *Journal of Quaternary Science* **27**(4): 371–382.

Elhatip H. 1997. The influence of karst features on environmental studies in Turkey. *Environmental Geology* **31**(1/2): 27–33.

Eris E, Wittenberg H. 2015. Estimation of baseflow and water transfer in karst catchments in Mediterranean Turkey by nonlinear recession analysis. *Journal of Hydrology* **530**: 500–507.

Eriş KK, Akçer Ön S, Çağatay MN, Ülgen UB, Ön ZB, Gürocak Z, Arslan TN, Akkoca DB, Damcı E, İnceöz M, Okan ÖÖ. 2018. Late Pleistocene to Holocene paleoenvironmental evolution of Lake Hazar, Eastern Anatolia, Turkey. *Quaternary International* **486**: 4–16.

Eroskay SO. 1982. Engineering properties of carbonate rocks and karst regions in Turkey. *Bulletin of the International Association of Engineering Geology* **25**: 61–65.

Faust D, Wolf D. 2017. Interpreting drivers of change in fluvial archives of the Western Mediterranean: a critical view. *Earth-Science Reviews* **174**: 53–83.

Finné M, Woodbridge J, Labuhn I, Roberts CN. 2019. Holocene hydro-climatic variability in the Mediterranean: a synthetic multi-proxy reconstruction. *The Holocene* **29**(5): 847–863.

Fleitmann D, Cheng H, Badertscher S, Edwards RL, Mudelsee M, Göktürk OM, Fankhauser A, Pickering R, Raible CC, Matter A, Kramers J, Tüysüz O. 2009. Timing and climatic impact of Greenland interstadials recorded in stalagmites from northern Turkey. *Geophysical Research Letters* **36**(19): 1–5, L19707.

Fryirs K. 2013. (Dis)Connectivity in catchment sediment cascades: a fresh look at the sediment delivery problem. *Earth Surface Processes and Landforms* **38**: 30–46.

Fryirs KA, Brierley GJ, Preston NJ, Kasai M. 2007. Buffers, barriers, and blankets: the (dis)connectivity of catchment-scale sediment cascades. *Catena* **70**: 49–67.

Fuchs M. 2007. An assessment of human versus climatic impacts on Holocene soil erosion in NE Peloponnese, Greece. *Quaternary Research* **67**(3): 349–356.

Fuchs M, Zöller L. 2006. Geoarchäologie aus geomorphologischer Sicht. Eine konzeptionelle Betrachtung. *Erdkunde* **60**: 139–146.

Fuchs M, Lang A, Wagner GA. 2004. The history of Holocene soil erosion in the Phlious Basin, NE Peloponnese, Greece, based on optical dating. *The Holocene* **14**(3): 334–345.

Fuchs M, Will M, Kunert E, Kreutzer S, Fischer M, Reverman R. 2011. The temporal and spatial quantification of Holocene sediment dynamics in a meso-scale catchment in northern Bavaria, Germany. *The Holocene* **21**(7): 1093–1104.

Geological Research Department. 2014. *Geological Maps of Turkey*, Sheets N40 and N41 (Şanliurfa), 1:100,000. General Directorate of Mineral Research and Exploration: Ankara.

Göktürk OM, Fleitmann D, Badertscher S, Cheng H, Edwards RL, Leuenberger M, Fankhauser A, Tüysüz O, Kramers J. 2011. Climate on the southern Black Sea coast during the Holocene: implications from the Sofular Cave record. *Quaternary Science Reviews* **30**: 2433–2445.

Greenfield HJ. 2010. The Secondary Products Revolution: the past, the present and the future. *World Archaeology* **42**(1): 29–54.

Grupe G, Peters J. 2011. Climate conditions, hunting activities and husbandry practices in the course of the Neolithic transition: the story told by stable isotope analysis of human and animal skeletal remains. In *Human Bioarchaeology of the Transition to Agriculture*, Pinhasi R, Stock JT (eds). Wiley-Blackwell: Chichester; 63–85.

Hammer EL, Arbuckle BS. 2017. 10,000 years of pastoralism in Anatolia: a review of evidence for variability in pastoral lifeways. *Nomadic Peoples* **21**(2): 214–267.

Harvey AM. 2002. Effective timescales of coupling within fluvial systems. *Geomorphology* **44**: 175–201.

Hoffmann T, Lang A, Dikau R. 2008. Holocene river activity: analysing ^{14}C-dated fluvial and colluvial sediments from Germany. *Quaternary Science Reviews* **27**: 2031–2040.

Houben P, Schmidt M, Mauz B, Stobbe A, Lang A. 2012. Asynchronous Holocene colluvial and alluvial aggradation: a matter of hydrosedimentary connectivity. *The Holocene* **23**: 544–555.

Jones AF, Macklin MG, Benito G. 2015. Meta-analysis of Holocene fluvial sedimentary archives: a methodological primer. *Catena* **130**: 3–12.

Jursa M. 2013. Agriculture, ancient Near East. In *The Encyclopedia of Ancient History*, Bagnall RS, Brodersen K, Champion CB, Erskine A, Huebner SR (eds). Wiley-Blackwell: Malden, UK; 208–210.

Keen-Zebert A, Tooth S, Rodnight H, Duller GAT, Roberts HM, Grenfell M. 2013. Late Quaternary floodplain reworking and the preservation of alluvial sedimentary archives in unconfined and confined river valleys in the eastern interior of South Africa. *Geomorphology* **185**: 54–66.

Knitter D, Braun R, Clare L, Nykamp M, Schütt B. 2019. Göbekli Tepe: a brief description of the environmental development in the surroundings of the UNESCO World Heritage Site. *Land* **8**(4): 1–16.

Kuzucuoğlu C. 2019. The physical geography of Turkey: an outline. In *Landscapes and Landforms of Turkey*, Kuzucuoğlu C, Çiner A, Kazancı N (eds). Springer: Cham, Switzerland; 7–15.

Kuzucuoğlu C, Çiner A, Kazancı N. 2019. The geomorphological regions of Turkey. In *Landscapes and Landforms of Turkey*, Kuzucuoğlu C, Çiner A, Kazancı N (eds). Springer: Cham, Switzerland; 41–178.

Lang A, Hönscheidt S. 1999. Age and source of colluvial sediments at Vaihingen–Enz, Germany. *Catena* **38**: 89–107.

Lewin J, Macklin MG. 2003. Preservation potential for Late Quaternary river alluvium. *Journal of Quaternary Science* **18**: 107–120.

Macklin MG, Johnstone E, Lewin J. 2005. Pervasive and long-term forcing of Holocene river instability and flooding in Great Britain by centennial-scale climate change. *The Holocene* **15**(7): 937–943.

Neef R. 2003. Overlooking the steppe-forest: a preliminary report on the botanical remains from early Neolithic Göbekli Tepe (southeastern Turkey). *Neo-Lithics* **2**: 13–16.

Notebaert B, Verstraeten G, Vandenberghe D, Marinova E, Poesen J, Govers G. 2011. Changing hillslope and fluvial Holocene sediment dynamics in a Belgian loess catchment. *Journal of Quaternary Science* **26**: 44–58.

Nykamp M, Knitter D, Schütt B. 2020a. Late Holocene geomorphodynamics in the vicinity of Göbekli Tepe, SE Turkey. *Catena* **195**: 1–14, 104759.

Nykamp M, Knitter D, Schütt B. 2020b. Sediment descriptions and geochemical analyses of radiocarbon-dated deposits from the vicinity of Göbekli Tepe: a dataset. *Data in Brief* **31**: 1–17, 106012.

Ön ZB, Akçer-Ön S, Özeren SM, Eriş KK, Greaves AM, Çağatay MN. 2018. Climate proxies for the last 17.3 ka from Lake Hazar (Eastern Anatolia), extracted by independent component analysis of μ-XRF data. *Quaternary International* **486**: 17–28.

Özcan H, Aydemir S, Çullu MA, Günal H, Eren M, Kadir S, Ekinci H, Everest T, Sungur A, FitzPatrick EA. 2018. Vertisols. In *The Soils of Turkey*, Kapur S, Akça E, Günal H (eds). Springer: Cham, Switzerland; 169–206.

Peng T, Wang S-J. 2012. Effects of land use, land cover and rainfall regimes on the surface runoff and soil loss on karst slopes in southwest China. *Catena* **90**: 53–62.

Peters J, Helmer D, von den Driesch A, Saña Segui M. 1999. Early animal husbandry in the northern Levant. *Paléorient* **25**: 27–48.

Peters J, Buitenhuis H, Grupe G, Schmidt K, Pöllath N. 2013. The long and winding road: ungulate exploitation and domestication in early Neolithic Anatolia (10000–7000 CAL BC). In *Origins and Spread of Domestic Animals in Southwest Asia and Europe*, Colledge S, Conolly J, Dobney K, Manning K, Shennan S (eds). Left Coast Press: Walnut Creek, CA; 83–114.

Peters J, Arbuckle BS, Pöllath N. 2014. Subsistence and beyond: animals in Neolithic Anatolia. In *The Neolithic in Turkey*, Özdo□an M, Başgelen N, Kuniholm P (eds), Vol. **6**. Archaeology and Art Publications: Istanbul; 135–203.

Peters J, Schmidt K, Dietrich L, Dietrich O, Pöllath N, Kinzel M, Clare L. 2019. Göbekli Tepe: agriculture and domestication. In *Encyclopedia of Global Archaeology*, Smith C (ed). Springer: Cham, Switzerland; 3065–3068.

Poeppl RE, Keesstra S, Maroulis J. 2017. A conceptual framework for understanding geomorphic change in human-impacted fluvial systems. *Geomorphology* **277**: 237–250.

Potts DT. 1997. *Mesopotamian Civilization. The Material Foundations*. Athlone Press: London.

Reimer PJ, Bard E, Bayliss A, Beck JW, Blackwell PG, Bronk Ramsey C, Buck CE, Cheng H, Edwards RL, Friedrich M, Grootes PM, Guilderson TP, Haflidason H, Hajdas I, Hatté C, Heaton TJ, Hoffmann DL, Hogg AG, Hughen KA, Kaiser KF, Kromer B, Manning SW, Niu M, Reimer RW, Richards DA, Scott EM, Southon JR, Staff RA, Turney CSM, van der Plicht J. 2013. IntCal13 and Marine13 radiocarbon age calibration curves 0–50,000 years cal BP. *Radiocarbon* **55**(4): 1869–1887.

Roberts N, Woodbridge J, Bevan A, Palmisano A, Shennan S, Asouti E. 2018. Human responses and non-responses to climatic variations

during the last Glacial–Interglacial transition in the eastern Mediterranean. *Quaternary Science Reviews* **184**: 47–67.

Roberts N, Woodbridge J, Palmisano A, Bevan A, Fyfe R, Shennan S. 2019a. Mediterranean landscape change during the Holocene: synthesis, comparison and regional trends in population, land cover and climate. *The Holocene* **29**(5): 923–937.

Roberts N, Allcock AL, Barnett H, Mather A, Eastwood WJ, Jones M, Primmer N, Yiğitbaşıoğlu H, Vannière B. 2019b. Cause-and-effect in Mediterranean erosion: the role of humans and climate upon Holocene sediment flux into a central Anatolian lake catchment. *Geomorphology* **331**: 36–48.

Rosen AM. 1997. The geoarchaeology of Holocene environments and land use at Kazane Höyük, S.E. Turkey. *Geoarchaeology* **12**(4): 395–416.

Scharpenseel HW, Schiffmann H. 1977. Soil radiocarbon analysis and soil dating. *Geophysical Surveys* **3**: 143–156.

Schumm SA. 1973. Geomorphic thresholds and complex response of drainage systems. In *Fluvial Geomorphology*, Morisawa M (ed). George Allen & Unwin: London; 299–310.

Schumm SA. 1991. *To interpret the earth: ten ways to be wrong*. Cambridge University Press: Cambridge, UK.

Shennan S, Downey SS, Timpson A, Edinborough K, Colledge S, Kerig T, Manning K, Thomas MG. 2013. Regional population collapse followed initial agriculture booms in mid-Holocene Europe. *Nature Communications* **4**: 1–8, 2486.

Sörensen L. 2007. *A spatial analysis approach to the global delineation of dryland areas of relevance to the CBD Programme of Work on Dry and Subhumid Lands*. UNEP-WCMC: Cambridge, UK.

Steadman SR, McMahon G. 2011. *The Oxford Handbook of Ancient Anatolia: (10,000-323 BCE)*. Oxford University Press: Oxford.

Tanno K-I, Willcox G. 2006. How fast was wild wheat domesticated? *Science* **311**(5769): 1886–1886.

Verstraeten G, Broothaerts N, Van Loo M, Notebaert B, D'Haen K, Dusar B, De Brue H. 2017. Variability in fluvial geomorphic response to anthropogenic disturbance. *Geomorphology* **294**: 20–39.

Walker M, Gibbard P, Head MJ, Berkelhammer M, Björck S, Cheng H, Cwynar LC, Fisher D, Gkinis V, Long A, Lowe J, Newnham R, Rasmussen SO, Weiss H. 2019. Formal subdivision of the Holocene Series/Epoch: a summary. *Journal of the Geological Society of India* **93**(2): 135–141.

Walsh K, Berger J-F, Roberts NC, Vanniere B, Ghilardi M, Brown AG, Woodbridge J, Lespez L, Estrany J, Glais A, Palmisano A, Finné M, Verstraeten G. 2019. Holocene demographic fluctuations, climate and erosion in the Mediterranean: a meta data-analysis. *The Holocene* **29**(5): 864–885.

Widell M, Studevent-Hickman B, Tenney J, Lauinger J, Mahoney D, Paulette T. 2013. Staple production, cultivation and sedentary life: model input data. In *Models of Mesopotamian Landscapes*, Wilkinson TJ, Gibson MG, Widell M (eds), BAR International Series 2552. Archaeopress: Oxford; 81–101.

Wilkinson TJ. 1990. *Town and Country in Southeastern Anatolia. Vol. I: Settlement and Land Use at Kurban Höyük and Other Sites in the Lower Karababa Basin*. University of Chicago Oriental Institute: Chicago, IL.

Williams AN. 2012. The use of summed radiocarbon probability distributions in archaeology: a review of methods. *Journal of Archaeological Science* **39**: 578–589.

Wolf D, Faust D. 2015. Western Mediterranean environmental changes: evidences from fluvial archives. *Quaternary Science Reviews* **122**: 30–50.

Yardımcı N. 2004. *Harran Ovası yüzey araştırması. Archaeological Survey in the Harran Plain*. Print A Grafik ve Matbaacılık: Istanbul.

Zolitschka B, Behre K-E, Schneider J. 2003. Human and climatic impact on the environment as derived from colluvial, fluvial and lacustrine archives: examples from the Bronze Age to the Migration period, Germany. *Quaternary Science Reviews* **22**: 81–100.

Supporting Information

Additional supporting information may be found online in the Supporting Information section at the end of the article.

Data S1. Supporting information

Data S2. Supporting information

Data S3. Supporting information

Data S4. Supporting information

